

NOVEL EVALUATION METHOD FOR NON-FOURIER EFFECTS IN HEAT PULSE EXPERIMENTS

A. FEHÉR¹, R. KOVÁCS¹²³

ABSTRACT. The heat pulse (flash) experiment is a well-known and widely accepted method to measure the thermal diffusivity of a material. In recent years, it is observed that the thermal behavior of heterogeneous materials can show deviation from the classical Fourier equation, resulting in a different thermal diffusivity and requiring further thermal parameters to identify. Such heterogeneity can be inclusions in metal foams, layered structure in composites, or even cracks and porous parts in rocks. Furthermore, the next candidate, the so-called Guyer-Krumhansl equation, is tested on these experiments with success. However, these recent evaluations required a computationally intensive fitting procedure using countless numerical solutions, even when a good initial guess for the parameters is found by hand. This paper presents a Galerkin-type discretization for the Guyer-Krumhansl equation, which helped us find a reasonably simple analytical solution for time-dependent boundary conditions. Utilizing this analytical solution, we developed a new evaluation technique to immediately estimate all the necessary thermal parameters using the measured temperature history.

1. INTRODUCTION

The engineering practice requires reliable ways to determine the necessary parameters, which are enough to characterize the material behavior. In what follows, we place our focus on the thermal description of materials, especially on heterogeneous materials such as rocks and foams. In recent papers [1, 2], it is reported that the presence of various heterogeneities can result in a non-Fourier heat conduction effect on macro-scale under room temperature conditions. A particular one is depicted in Fig. 1 for a capacitor sample having a periodic layered structure. Such effects are observed in a so-called flash (or heat pulse) experiment in which the front side of the specimen is excited with a short heat pulse, and the temperature is measured at the rear side. That temperature history is used to find the thermal diffusivity in order to characterize the transient material behavior.

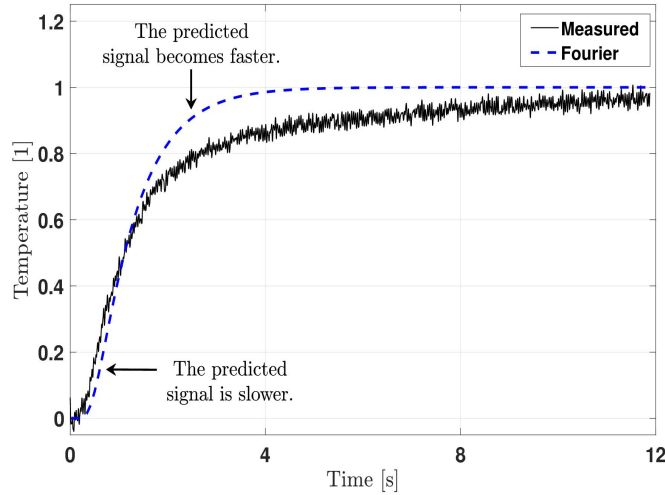


FIGURE 1. Measured rear side temperature history for the capacitor sample and the prediction provided by Fourier's theory.

This non-Fourier effect occurs on a specific time interval as Fig. 1 shows for a typical outcome of the flash experiments; this is called over-diffusion. After that interval, the Fourier equation appears to be a suitable choice for modeling, the influence of the heterogeneities vanishes (later, we show further examples). Also, there is no difference

between the steady-states of Fourier and non-Fourier heat equations. Based on our experimental experience, the existence of over-diffusion depends on various factors, for instance, sample thickness, characteristic parallel time scales, and excitation (i.e., boundary conditions) [3].

In the following sections, we organize the discussion as follows. First, we briefly introduce the two heat conduction models to model the heat pulse experiments and used for evaluations with a particular set of dimensionless quantities. Second, we shortly present how the complete evaluation with the Fourier heat equation can be conducted. Then, we move on the way of the evaluation procedure with the Guyer-Krumhansl equation. After, we demonstrate the benefits of this fitting procedure and revisit some previous measurements. Furthermore, we decided to place the derivation of the analytical solutions to the end of the paper as an Appendix. According to our knowledge, the Galerkin method has not been used before for the Guyer-Krumhansl equation, and is a novel result in this respect, we want to keep the focus on its practical utilizations.

2. MODELS FOR HEAT PULSE EXPERIMENTS

Although numerous generalizations of Fourier's law exist in the literature [4], there is solely one of them, which indeed proved to be reasonable as the next candidate beyond Fourier's theory, this is called Guyer-Krumhansl (GK) equation, this constitutive equation reads in one spatial dimension

$$\tau_q \partial_t q + q + \lambda \partial_x T - \kappa^2 \partial_{xx} q = 0. \quad (1)$$

Here, τ_q is the relaxation time for the heat flux q and κ^2 is a kind of 'dissipation parameter', usually related to the mean free path. Whereas it was first derived on the basis of kinetic theory [5], this model also has a strong background in non-equilibrium thermodynamics with internal variables (NET-IV) [6, 7]. While in the first case, one assumes an underlying mechanism for phonons as the kinetic theory requires it, this is entirely neglected in the case of NET-IV, leaving the coefficients to be free (however, their sign is restricted by the II. law of thermodynamics). Eq. (1) is a time evolution equation for the heat flux, and in order to have a mathematically and physically complete system, we need the balance of internal energy e , too,

$$\rho c \partial_t T + \partial_x q = 0, \quad (2)$$

in which the equation of state $e = cT$ is used with c being the specific heat and ρ is the mass density. All these coefficients are constant, only rigid bodies are assumed with no heat source.

At this point, we owe an explanation of why we leave the Maxwell-Cattaneo-Vernotte (MCV) equation out of sight.

- (1) Hyperbolicity vs. parabolicity. It is usually claimed that a heat equation model should be hyperbolic such as the MCV theory, describing finite propagation speed. Indeed, this seems reasonable, but it does not help in the practical applications under common conditions (room temperature, heterogeneous materials). The Fourier equation is still well-applicable in spite of its parabolic nature, therefore we do not see it as a decisive property.
- (2) In a low-temperature situation, the MCV model was useful, primarily due to the observed wave phenomenon in super-fluids, called second sound [8, 9]. Despite the GK equation's parabolic nature, it also helped the researchers find the second sound in solids as well [10].
- (3) There is a significant effort to find the trace of wave propagation at room temperature (in a macro-scale object, so nano-structures does not count now), sadly with no success [11, 12].
- (4) There are higher-order models as well, such as ballistic-diffusive models [13–15], but they are related to a different research program, and for this work, investigating macro-scale objects, they do not seem relevant.
- (5) On the analogy of the MCV model, the so-called dual-phase lag (DPL) equation [16] usually used in many works as the best candidate after Fourier's law. Sadly, this model introduces two time constants in an ad hoc manner, violating basic physical principles [17, 18], leading to mathematically ill-posed problems as well [19, 20].

Last but not least, we also must mention a relatively less-known model from the literature, the Nyíri equation [21],

$$q + \lambda \partial_x T - \kappa^2 \partial_{xx} q = 0, \quad (3)$$

which one is indeed similar to the Guyer-Krumhansl model but leaves the time lagging effects out of sight, hence it is purely a spatially nonlocal heat equation. Testing its solutions with the method presented in the Appendix, it turned out to be inaccurate for measurements, unfortunately. Consequently, the GK model is indeed the simplest but necessary extension for the Fourier equation, neither the MCV nor the Nyíri models are capable of describing these experiments accurately. In other words, the two new parameters (τ_q and κ^2) are truly needed.

2.1. T and q-representations. Depending on the purpose, it is useful to keep in mind that for such linear models, it is possible to chose a ‘primary’ field variable, which could ease the definition of boundary conditions in some cases. For the GK equation, the temperature T and the heat flux q are the candidates, and their forms are

$$\text{T-representation: } \tau_q \partial_{tt} T + \partial_t T - \alpha \partial_{xx} T - \kappa^2 \partial_{txx} T = 0, \quad (4)$$

$$\text{q-representation: } \tau_q \partial_{tt} q + \partial_t q - \alpha \partial_{xx} q - \kappa^2 \partial_{txx} q = 0. \quad (5)$$

We note that in T -representation, it is unknown how to define boundary condition for q since it requires knowledge on $\partial_{xx} q$. On the other hand, in q -representation, it becomes meaningless to speak about T -boundaries. In a previous analytical solution for the GK equation [22], this difference was inevitable to realize. In the present work, we use the system (1)-(2). It is also interesting to notice that the GK model can recover the solution of the Fourier equation when $\kappa^2/\tau_q = \alpha$, this is called Fourier resonance [1, 23]. Overall, the coefficients τ_q , α , and κ^2 must be fitted to the given temperature history.

2.2. Dimensionless set of parameters. Following [1], we introduce these definitions for the dimensionless parameters (quantities with hat):

$$\begin{aligned} \text{time:} & \quad \hat{t} = \frac{t}{t_p} \quad \text{and} \quad \hat{x} = \frac{x}{L}; \\ \text{thermal diffusivity:} & \quad \hat{\alpha} = \frac{\alpha t_p}{L^2} \quad \text{with} \quad \alpha = \frac{\lambda}{\rho c}; \\ \text{temperature:} & \quad \hat{T} = \frac{T - T_0}{T_{\text{end}} - T_0} \quad \text{with} \quad T_{\text{end}} = T_0 + \frac{\bar{q}_0 t_p}{\rho c L}; \\ \text{heat flux:} & \quad \hat{q} = \frac{q}{\bar{q}_0} \quad \text{with} \quad \bar{q}_0 = \frac{1}{t_p} \int_0^{t_p} q_0(t) dt; \\ \text{heat transfer coefficient:} & \quad \hat{h} = h \frac{t_p}{\rho c}; \end{aligned} \quad (6)$$

together with $\hat{\tau}_q = \frac{\tau_q}{t_p}$, $\hat{\kappa}^2 = \frac{\kappa^2}{L^2}$, where \hat{t} differs from the usual Fourier number in order to decouple the thermal diffusivity from the time scale in the fitting procedure. Furthermore, t_p denotes the constant heat pulse duration for which interval \bar{q}_0 averages the heat transferred with the heat pulse defined by $q_0(t)$. Here, L is equal with the sample thickness. T_{end} represents the adiabatic steady-state, and T_0 is the uniform initial temperature. In the rest of the paper, we shall omit the hat notation, otherwise we add the unit for the corresponding quantity. Utilizing this set of definitions, one obtains the dimensionless GK model:

$$\begin{aligned} \partial_t T + \partial_x q &= 0, \\ \tau_q \partial_t q + q + \alpha \partial_x T - \kappa^2 \partial_{xx} q &= 0. \end{aligned} \quad (7)$$

The initial condition is zero for both fields. For further details, we refer to the Appendix in which we present the analytical solution for the two heat equations. This set of dimensionless parameters does not change the definition of the Fourier resonance condition, i.e., it remains $\hat{\kappa}^2/\hat{\tau}_q = \hat{\alpha}$.

3. EVALUATION WITH THE FOURIER THEORY

The analytical solution of the Fourier equation is found for the rear side in the form of

$$T(x=1, t) = Y_0 \exp(-ht) - Y_1 \exp(x_F t), \quad x_F = -2h - \alpha \pi^2, \quad t > 30, \quad (8)$$

where all the coefficients are expressed in detail in the Appendix. First, we must estimate the heat transfer coefficient h by choosing arbitrarily two temperature values at the decreasing part of temperature history. In this region, $\exp(x_F t) \approx 0$, thus

$$h = -\frac{\ln(T_2/T_1)}{t_2 - t_1}. \quad (9)$$

For the Fourier theory, it is possible to express the thermal diffusivity explicitly, i.e.,

$$\alpha_F = 1.38 \frac{L^2}{\pi^2 t_{1/2}}, \quad (10)$$

and after registering $t_{1/2}$, it can be directly determined. This is the ratio of the thermal conductivity λ and the specific heat capacity ρc . Then, the top of the temperature history (T_{max}) follows by reading the time instant (t_{max}) when T_{max} occurs. Figure 2 schematically summarizes this procedure. Overall, we obtained the heat transfer coefficients, the thermal diffusivity and T_{max} , which all used for the Guyer-Krumhansl theory.

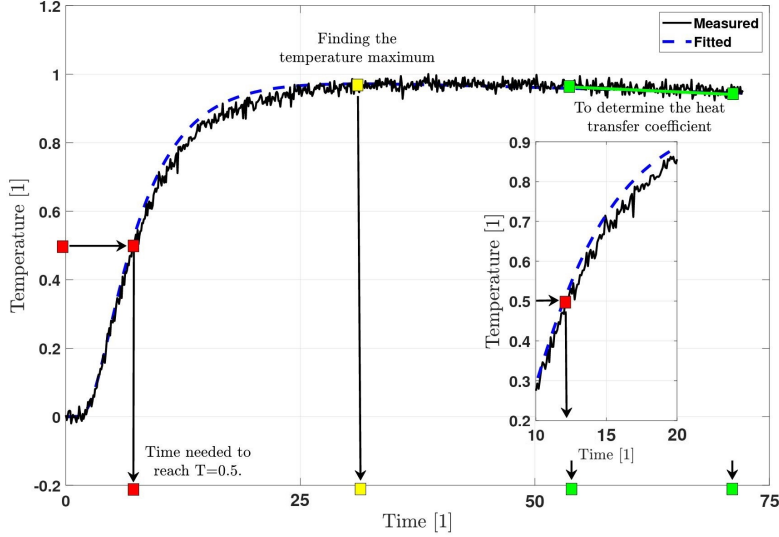


FIGURE 2. Schematically presenting the evaluation method using Fourier's theory.

4. EVALUATION WITH THE GUYER-KRUMHANSL THEORY

The situation here becomes more difficult since this non-Fourier theory consists of two ‘time constants’ (x_1 and x_2) instead of one (x_F in the Fourier theory). Consequently, it is not possible to find these exponents without making simplifications, in which one must be immensely careful. We prepared ‘parameter maps’ for all possible τ_q and κ^2 values that could be practically possible and beyond in order to check the effect of the simplifications made in the following. However, we still had to restrict ourselves to a domain, which is $3 > \kappa^2/(\alpha\tau_q) \geq 1$. Its lower limit expresses the Fourier case, and any other combination falls on the over-diffusive region. The highest experimentally observed ratio so far is around 2.5, thus we expect 3 to be eligible. For κ^2 , we consider $0.02 < \kappa^2 < 1$. We want to emphasize that the GK theory itself is not restricted on this domain, it would allow under-diffusive (‘wave-like’) propagation as well [10]. However, for the present situation, we consider it out of interest in the lack of experimental observation for room temperature experiments on macro-scale heterogeneous samples. In the GK theory, we can express the rear side temperature history as

$$T(x=1, t) = Y_0 \exp(-ht) - Z_1 \exp(x_1 t) - Z_2 \exp(x_2 t), \quad x_1, x_2 < 0, \quad (11)$$

for the detailed calculation and parameter definitions, we refer to the Appendix again. This can be equivalently formulated realizing that $Z_2 = -P_0 - Z_1$,

$$T(x=1, t) = Y_0 \exp(-ht) - Z_1 (\exp(x_1 t) - \exp(x_2 t)) + P_0 \exp(x_2 t), \quad (12)$$

where merely one simplification becomes possible for all τ_q and κ^2 : $\exp(x_1 t) \gg \exp(x_2 t)$ when $t > 60$, i.e.,

$$T(x=1, t > 60) = Y_0 \exp(-ht) - Z_1 \exp(x_1 t) + P_0 \exp(x_2 t). \quad (13)$$

This form is more advantageous because P_0 remains practically constant for a given boundary condition, thus its value can be assumed a-priori, this is exploited in the evaluation method. Now, let us present from step by step the determination of GK parameters, depicted on Fig. 3.

- Step 1/A. We have to observe that the temperature predicted by Fourier's theory always runs together with the measured one at the beginning, after that, it rises faster at the top. In other words, in this region the same temperature value (usually around 0.7 – 0.95) is reached sooner. Mathematically, we can express it by formally writing the equations for the Fourier and GK theories as follows,

$$T_F = Y_0 \exp(-ht) - Y_1 \exp(x_F t_F); \quad T_{GK} = Y_0 \exp(-ht_m) - Z_1 \exp(x_1 t_m) + P_0 \exp(x_2 t_m), \quad (14)$$

where the t_F time instant is smaller than the measured t_m , also $T_F = T_{GK}$ holds. Let us choose such two temperatures arbitrarily and taking their ratio, it yields

$$\exp(x_F(t_{F1} - t_{F2})) = \exp(x_1(t_{m1} - t_{m2})) \frac{-Z_1 + P_0 \exp((x_2 - x_1)t_{m1})}{-Z_1 + P_0 \exp((x_2 - x_1)t_{m2})} \quad (15)$$

where the fraction on the right hand side is close to 1, mostly between 1 and 1.05 for ‘small’ time intervals. It could be possible to introduce it as a correction factor (denoted with c below) for x_1 in an iterative procedure if more to be known about τ_q and κ^2 . After rearrangement, we obtain a closed form formula for x_1 :

$$x_1 = \frac{\ln(1/c)}{t_{m1} - t_{m2}} + x_F \frac{t_{F1} - t_{F2}}{t_{m1} - t_{m2}}. \quad (16)$$

Taking $c = 1$ is equivalent with neglecting $\exp(x_2 t)$ from the beginning around reaching T_{\max} , and leading to this same expression. Eventually, it introduces a correction for the Fourier exponent x_F based on the deviation from the measured data with the possibility to apply further corrections using c if needed. Practically, we take the 80% and 90% of T_{\max} and for the next 20 subsequent measurement points, then we consider their mean value to be x_1 . From mathematical point of view, closer data point pairs should perform better, but it does not due to the uncertainty in the measurement data. According to our experience, it offers a more consistent value for x_1 .

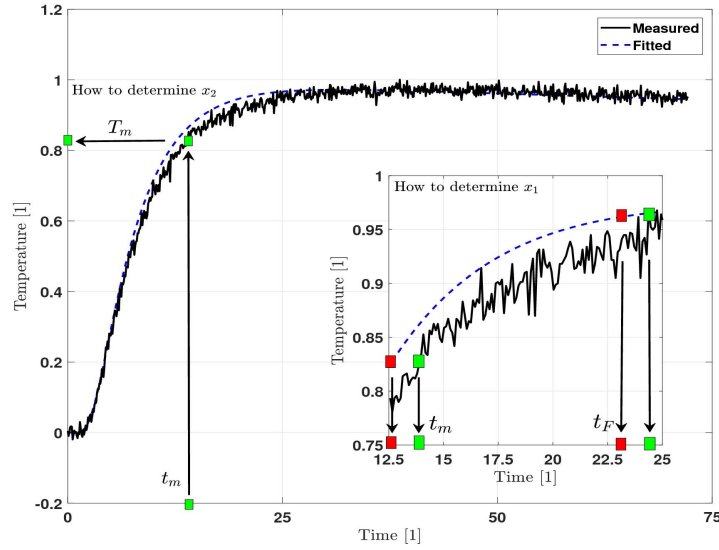


FIGURE 3. The schematic representation of the evaluation method using the Guyer-Krumhansl theory. Here, the ‘fitted curve’ belongs to the Fourier equation.

- Step 1/B. In parallel with part A, we can determine the coefficient Z_1 for each t_m and for each corresponding $x_{1,m}$, that is,

$$Z_{1,m} = \exp(-x_{1,m} t_m) (T_m - Y_0 \exp(-h t_m)) \quad (17)$$

where the subscript m denotes the value related to one measurement point. Also, after 20 subsequent points, we take the mean value of the set $\{Z_{1,m}\}$.

- Step 2. At this point, we can exploit that P_0 is ‘almost constant’, i.e., $2 < -P_0 < 2.03$ holds. Here, 2.03 comes from the parameter sweep, we did not observe higher values for $-P_0$, and also, it cannot be smaller than 2. This property allows us to a-priori assume its value (such as $P_0 = -2.015$), and in a later step, we must fine-tune since the overall outcome reacts sensitively. Using P_0 , we can obtain $Z_2 = -P_0 - Z_1$. In order to obtain x_2 , we can rearrange the equation

$$T = Y_0 \exp(-h t) - Z_1 \exp(x_1 t) - Z_2 \exp(x_2 t) \quad (18)$$

for x_2 , and calculate it as a mean value of the set $\{x_{2,m}\}$ filled with values related to each t_m . When having noisy data, this approach can result in positive x_2 values, unfortunately. These values must be excluded, otherwise, it leads to instability and a meaningless outcome. Careful data filtering can help to solve this shortcoming, and in fact, we used it to ease the calculation (the details are plotted in the next section).

- Step 3. Now, having both exponents and coefficients, it is possible to rearrange the analytical expressions to the GK parameters explicitly and calculate α_{GK} , τ_q and κ^2 :

$$x_1, x_2 \Rightarrow k_1, k_2; \quad Z_1 \Rightarrow DP_0 \Rightarrow M_1, M_2 \Rightarrow \tau_q \Rightarrow \alpha_{GK} \Rightarrow \kappa^2. \quad (19)$$

For the detailed parameter definitions, we refer to the Appendix.

- Step 4. As it is mentioned in Step 2, the overall outcome is sensitive to P_0 . Therefore we choose to make a sweep on the possible interval with the step of 0.002, producing the temperature history for each set of parameters and characterizing them with R^2 , the coefficient of determination. Lastly, we chose the best set.

Practically, this evaluation method reduces the number of ‘fitted’ parameters as only P_0 has to be fine-tuned at the end. Besides, it is constrained into a relatively narrow range, consequently, the overall evaluation procedure takes only a few seconds instead of hours to perform computationally intensive algorithms.

5. COMPARISON WITH FOREGOING EXPERIMENTS

First, we revisit the experiments presented in [3] since that set of data on Basalt rock samples with thicknesses of 1.86, 2.75 and 3.84 mm, showed size dependence both on the thermal diffusivity and on the non-Fourier effects. However, the fitted parameters in [3] found by hand, thus not exactly precise. Here, we aim to specify the exact quantities for the GK model and establishing a more robust theoretical basis for the observations. Second, we reevaluate the data recorded on a metal foam sample with 5.2 mm thickness. This belongs to the samples showing the potent non-Fourier effect, presented first in [2]. Figure 4 shows these samples.

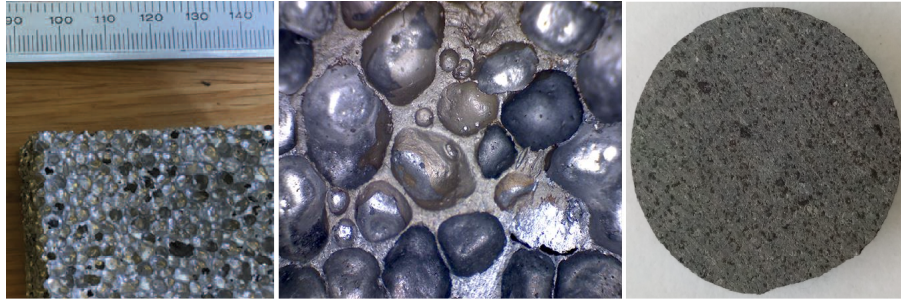


FIGURE 4. The magnified view of the metal foam specimen (center) and the basalt rock sample (right).

In some cases, the available data is too noisy for such an evaluation method, an example is presented in Fig. 5. That data is smoothed using the built-in Savitzky-Golay algorithm of Matlab. Besides, we paid much attention to not smooth it overly in order to keep the physical content untouched as much as possible.

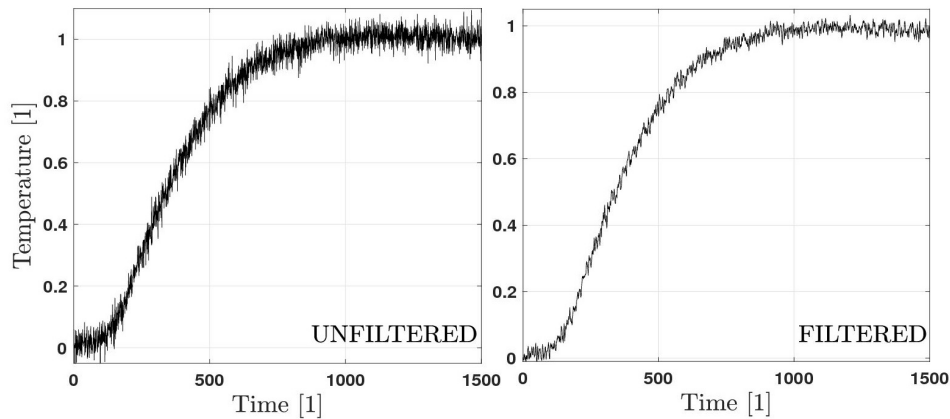


FIGURE 5. The effect of data smoothening, using 10 neighboring points in the Savitzky-Golay algorithm.

5.1. Basalt rock samples. Regarding the exact details of measurements, we refer to [3]. Tables 1 and 2 consist of our findings using this evaluation algorithm. Comparing the outcomes of the two fitting procedures, we find the thermal diffusivities to be close to each other. However, this is not the case with the GK parameters τ_q and κ^2 , they significantly differ from the previous values from [3]. Despite the huge difference, the size-dependence for both the Fourier and non-Fourier behaviors is apparent nevertheless. The fitted temperature histories are depicted in Figs. 6, 7, 8 and 9 for each thickness, respectively. Each figure shows the R^2 value for the fitted curve. For the Fourier one, two of them are given: R_t^2 represents the one found without any fine-tuned thermal diffusivity, this is purely theoretical. The other R^2 stands for fine-tuned α_F .

In the first case ($L = 1.86$ mm), although the difference for the non-Fourier samples seems negligible, it results in 10% difference in the thermal diffusivity. It is more visible from Table 2, in which the Fourier resonance condition spectacularly characterize the deviation from Fourier's theory, it decreases for thicker samples. Regarding the third one ($L = 3.84$ mm), Fourier's theory seems to be 'perfectly splendid', and the GK model hardly improves it. Indeed, the 0.94 for the Fourier resonance is close enough to 1 to consider it to be a Fourier-like propagation.

Basalt rock samples	Findings in [3]				Refined results			
	α_F	α_{GK}	τ_q	κ^2	α_F	α_{GK}	τ_q	κ^2
	10^{-6} [m ² /s]	10^{-6} [m ² /s]	[s]	10^{-6} [m ²]	10^{-6} [m ² /s]	10^{-6} [m ² /s]	[s]	10^{-6} [m ²]
1.86 mm	0.62	0.55	0.738	0.509	0.68	0.61	0.211	0.168
2.75 mm	0.67	0.604	0.955	0.67	0.66	0.61	0.344	0.268
3.84 mm	0.685	0.68	0.664	0.48	0.70	0.68	1	0.65

TABLE 1. Summarizing the fitted thermal parameters.

$\frac{\kappa^2}{\tau_q \alpha}$	Findings in [3]	Refined values
1.86 mm	1.243	1.295
2.75 mm	1.171	1.272
3.84 mm	1.06	0.94

TABLE 2. Characterizing the non-Fourier behavior using the Fourier resonance condition.

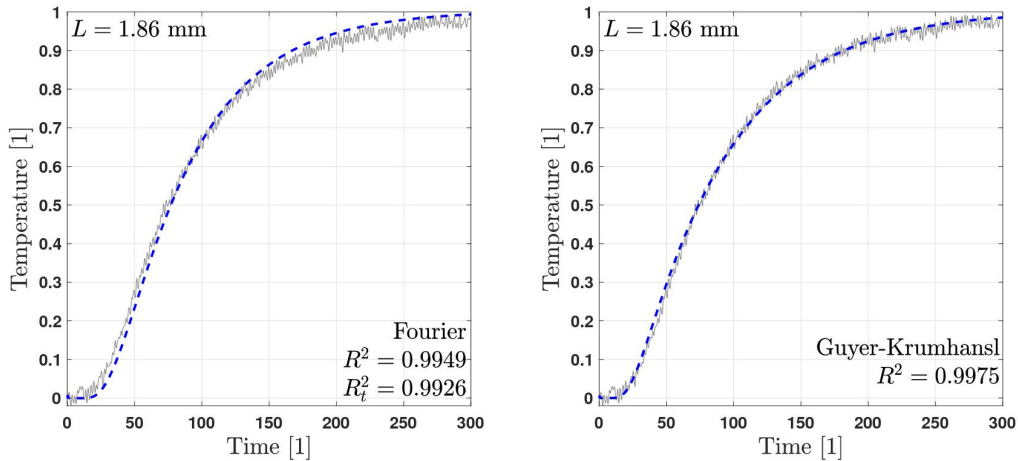


FIGURE 6. The rear side temperature history for the basalt rock sample with $L = 1.86$ mm.

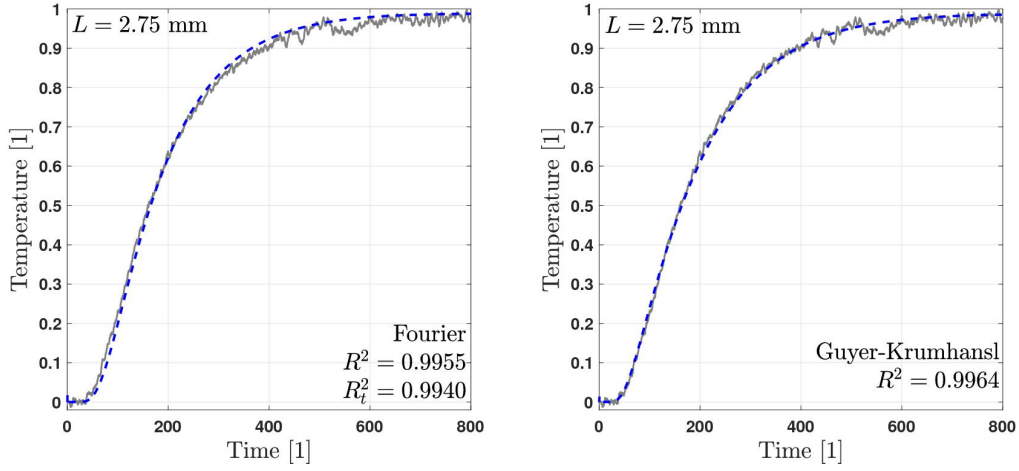


FIGURE 7. The rear side temperature history for the basalt rock sample with $L = 2.75$ mm.

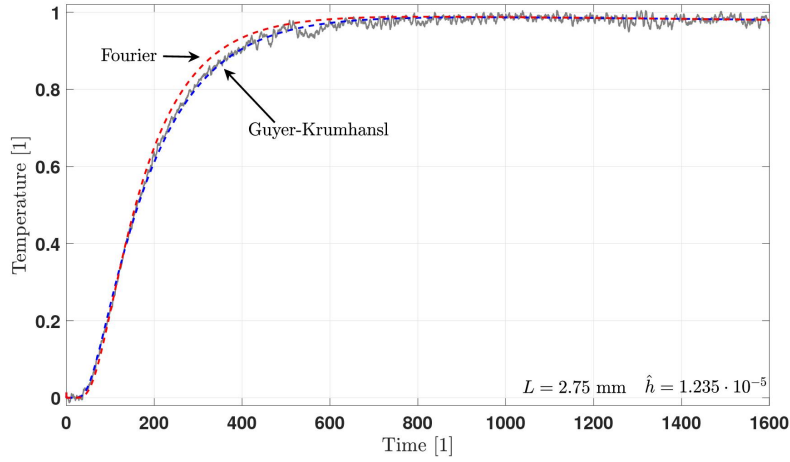


FIGURE 8. Demonstrating the complete fitting for the rear side temperature in case of the basalt rock sample with $L = 2.75$ mm.

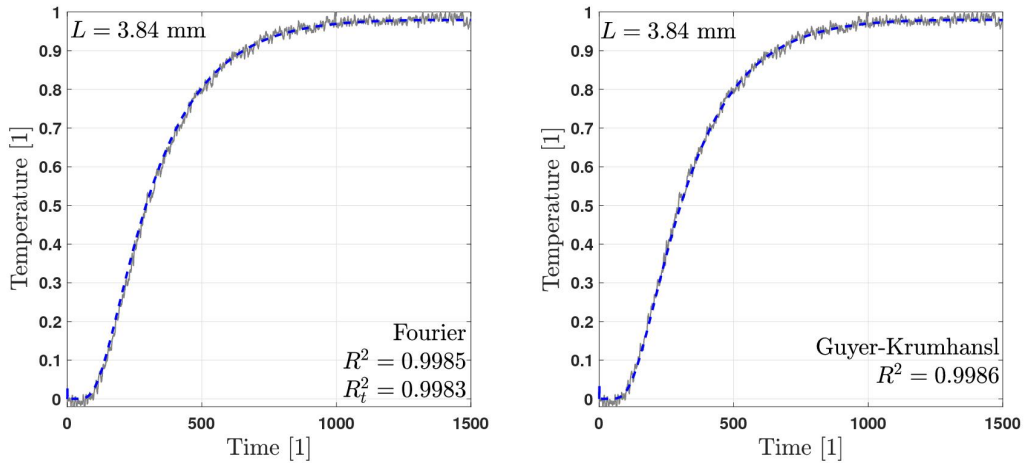


FIGURE 9. The rear side temperature history for the basalt rock sample with $L = 3.84$ mm.

5.2. Metal foam. Regarding the extent of the non-Fourier effect, the situation becomes remarkably different for the metal foam sample, presented first in [2]. The millimeter size inclusions can significantly influence the thermal behavior. The outcome is plotted in Fig. 10 together with the corresponding R^2 values. Table 3 helps to compare the fitted values found by Wolfram Mathematica to ours. Notwithstanding that the GK parameters are in correspondence, the most notable difference is on the thermal diffusivities, interestingly. The Fourier resonance parameter is found to be 2.395 with our procedure, while on the contrary to 3.04 in [2]. Common in both cases, the ratio of α_F and α_{GK} is found to be 1.28-1.29, which represents an indeed remarkable deviation from Fourier's theory.

Metal foam sample	Findings in [2] with Wolfram Math				Present algorithm			
	α_F	α_{GK}	τ_q	κ^2	α_F	α_{GK}	τ_q	κ^2
	$10^{-6} \text{ [m}^2/\text{s]}$	$10^{-6} \text{ [m}^2/\text{s]}$	$[\text{s}]$	$10^{-6} \text{ [m}^2]$	$10^{-6} \text{ [m}^2/\text{s]}$	$10^{-6} \text{ [m}^2/\text{s]}$	$[\text{s}]$	$10^{-6} \text{ [m}^2]$
5.2 mm	3.04	2.373	0.402	2.89	3.91	3.01	0.304	2.203

TABLE 3. Summarizing the fitted thermal parameters for the metal foam sample.

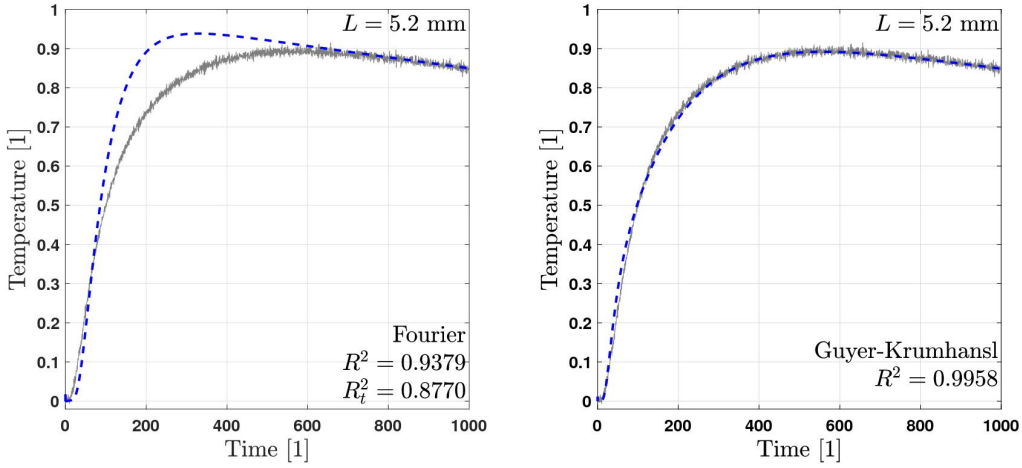


FIGURE 10. The rear side temperature history for the metal foam sample with $L = 5.2$ mm.

6. DISCUSSION AND SUMMARY

We developed an algorithm to efficiently evaluate room temperature heat pulse experiments in which a non-Fourier effect could exist. This is called over-diffusive propagation and detunes the thermal diffusivity, even when the deviation is seemingly small or negligible for the rear side temperature history. The presented method is based on the analytical solution of the Guyer-Krumhansl equation, including temperature-dependent convection boundary condition, thus the heat transfer to the environment can be immediately included in the analysis. The reevaluation of preceding experiments showed a real size-dependence for all thermal parameters, especially for the GK coefficients τ_q and κ^2 . Furthermore, it is in accordance with the result of the iterative ‘brute force’ iterative fitting procedure of Wolfram Math, basically, but using much less computational resource.

We plan to improve this procedure by including the investigation of front side temperature history, too. When x_1 is obtained from the rear side, it could be easily used to describe the front side's thermal behavior. This is much more sensitive to the initial time evolution right after the excitation, therefore it could serve as a better candidate to achieve a more precise and robust estimation for the x_2 exponent. Also, having two temperature histories would be a remarkable step forward to ascertain the existence of non-Fourier heat conduction.

We believe that this procedure lays the foundations for the more practical engineering applications of non-Fourier models, especially for the best candidate among all of them, the Guyer-Krumhansl equation. It sheds new light on the classical and well-known flash experiments, and we provide the necessary tools to find additional thermal parameters to achieve a better description of heterogeneous materials. It becomes increasingly important with the spreading of composites and foams and helps characterize 3D printed samples with various inclusions.

7. ACKNOWLEDGEMENT

The authors thank Tamás Fülöp, Péter Ván, and Mátyás Szücs for the valuable discussions. We thank László Kovács (Kőmérő Kft., Hungary) and Tamás Bárczy (Admatis Kft.) for producing the rock and metal foam samples.

The research reported in this paper and carried out at BME has been supported by the grants National Research, Development and Innovation Office-NKFIH FK 134277, and by the NRDI Fund (TKP2020 NC, Grant No. BME-NC) based on the charter of bolster issued by the NRDI Office under the auspices of the Ministry for Innovation and Technology. This paper was supported by the János Bolyai Research Scholarship of the Hungarian Academy of Sciences.

8. APPENDIX: GALERKIN-TYPE SOLUTION OF HEAT EQUATIONS

Since the non-Fourier models are not well-known in the general literature, there are only a few available analytical and numerical methods to solve such a spatially nonlocal equation like the Guyer-Krumhansl one. The nonlocal property is a cornerstone of these models since the usual boundary conditions do not work in the same way. That could be a problem when the outcome seemingly violates the maximum principle, see for instance [24] in which the operational approach is applied [25].

Another particular candidate originates from the spectral methods, it is called Galerkin method, where both the weight and the trial functions are the same. Fortunately, following [22], we can surely apply sine and cosine trial functions in which terms the solution can be expressed. It is important to emphasize that we deal with a system of partial differential equations in our case. The physical (and mathematical) connection between the field variables restricts the family of trial functions. Namely, even in the simplest case of the Fourier heat equation,

$$\partial_t T + \partial_x q = 0, \quad q + \alpha \partial_x T = 0, \quad (20)$$

q and T are orthogonal to each other, and the trial functions must respect this property. Our choice is found by the method called separation of variables, but it resulted in a too complicated outcome due to the time-dependent boundary condition. In [22], the heat pulse is modeled with a smooth $q_0(t) = 1 - \cos(2\pi t/t_p)$ function on the $0 < t \leq t_p$ interval. It is disadvantageous since the most interesting part falls beyond t_p , and the solution in $t_p < t$ must account for the state at the time instant t_p as an initial condition. Therefore, it results in cumbersome expressions for the coefficients.

We overcome this difficulty by introducing a different function to model the heat pulse, i.e., we use $q_0(t) = -(\exp(-C_1 t) + \exp(-C_2 t))/n$, where C_1 and C_2 are chosen to have a sufficiently small q_0 after t_p , hence the values are $C_1 = 1/0.075$ and $C_2 = 6$. The coefficient n is normalizing q_0 to 1 from 0 to t_p , so it is $n = (C_1 - C_2)/(C_1 C_2)$. For larger time instants, the front side becomes adiabatic. Regarding the rear side boundary condition, we choose to account heat convection for both models.

- (1) First, we restrict ourselves to the Fourier equation. According to our previous experiments [1–3], one can safely use the Fourier equation where cooling effects become significant. This solution is used to estimate the heat transfer coefficient, the maximum temperature and give a first approximation to the thermal diffusivity.
- (2) In the second step, we repeat the calculation for the GK model with the same boundary conditions. We use the previously found Fourier parameters as the input to estimate the GK parameters and fine-tune the thermal diffusivity. The heat transfer coefficient and the temperature maximum can be kept the same.

8.1. Step 1: solving the Fourier equation. While there are several available solutions in the literature, we want to see how the Galerkin approach performs on this model using our set of dimensionless parameters and boundary conditions. Consequently, we can keep our findings to be consistent between the two heat equation models. Let us recall the mathematical model for the sake of traceability. In the Fourier model, we have

$$\partial_t T + \partial_x q = 0, \quad q + \alpha \partial_x T = 0, \quad (21)$$

with

$$q_0(t) = -\frac{1}{n} \left(\exp(-C_1 t) + \exp(-C_2 t) \right), \quad n = \frac{C_1 - C_2}{C_1 C_2}, \quad q_1(t) = hT(x = 1, t), \quad (22)$$

in which all parameters are dimensionless as presented in Sec. 2.2. The initial conditions are $q(x, t = 0) = 0$ and $T(x, t = 0) = 0$, the conducting medium is thermally relaxed. We emphasize that one does not need to separately specify boundary conditions for the temperature field T as well. Regarding the heat flux field q , we must separate the time-dependent part from the homogeneous one,

$$q(x, t) = w(x, t) + \tilde{q}(x, t), \quad w(x, t) = q_0(t) + x(q_1(t) - q_0(t)) \quad (23)$$

with \tilde{q} being the homogeneous field and w inherits the entire time-dependent part from the boundary (and x runs from 0 to 1). The spectral decomposition of \tilde{q} and T are

$$\tilde{q}(x, t) = \sum_{j=1}^N a_j(t) \phi_j(x), \quad T(x, t) = \sum_{j=1}^N b_j(t) \varphi_j(x), \quad (24)$$

with $\phi_j(x) = \sin(j\pi x)$ and $\varphi_j(x) = \cos(j\pi x)$. Revisiting the boundary conditions, q_0 is trivial, and q_1 becomes: $q_1(t) = hT(x = 1, t) = h \sum_{j=0}^N b_j(-1)^j$. Naturally, one has to represent also $w(x, t)$ in the space spanned by $\phi_j(x)$. Once one substituted these expressions into (21), multiplied them by the corresponding weight functions and integrated respect to x from 0 to 1, one obtains a system of ordinary differential equations (ODE). Here, we exploit that the square of the trial functions $\phi(x)^2$ and $\varphi(x)^2$ are both integrable and after integration they are equal to $1/2$. Since the cos series have a non-zero part for $j = 0$, we handle it separately from the others corresponding to $j > 0$.

- For $j = 0$, we have

$$\dot{b}_0 + \partial_x w = 0, \rightarrow \dot{b}_0 = -hb_0 + q_0 \quad (25)$$

with the upper dot denoting the time derivative, and $a_0 = 0$ identically.

- For $j > 0$, we obtained

$$\dot{b}_j + j\pi a_j = 0, \quad (26)$$

$$a_j = \alpha j\pi b_j + \frac{2}{j\pi}(hb_j - q_0), \quad (27)$$

where the term $2/(j\pi)$ comes from the sin series expansion of w . We note that for $j > 0$, $\partial_x w$ does not contribute to the time evolution.

Such ODE can be solved easily both numerically and analytically for suitable q_0 functions. Figure 11 shows the analytical solution programmed in Matlab in order to demonstrate the convergence to the right (physical) solution. In this respect, we refer to [26] in which a thorough analysis is presented on the analytical and numerical solution of heat equations beyond Fourier. Our interest is to utilize as less terms as possible of the infinite series, which is able to properly describe the rear side temperature history (i.e., the measured one) from a particular time instant. In other words, we want to simplify the complete solution as much as possible but keeping its physical meaning.

Starting with $j = 0$ case, we find that the terms in the particular solution with $\exp(-C_1 t)$ and $\exp(-C_2 t)$ extinct very quickly, thus we can safely neglect them with keeping the $\exp(-ht)$ as the leading term throughout the entire time interval we investigate. Briefly, $j = 0$ yields

$$b_0(t) = Y_0 \exp(-ht), \quad Y_0 = (C_1 - C_2)/(n(C_1 - h)(C_2 - h)). \quad (28)$$

Continuing with $j = 1$, we make the same simplifications and neglecting the same exponential terms as previously after taking into account the initial condition, and we found

$$b_1(t) = Y_1 \exp(-2ht) \exp(-\pi^2 t), \quad Y_1 = 2(C_1 - C_2)/(n(C_1 + x_F)(C_2 + x_F)), \quad x_F = -2h - \alpha\pi^2. \quad (29)$$

Based on the convergence analysis (Fig. 11), we suppose that these terms are eligible to properly describe the temperature history after $t > 30$ (which is equal to 0.3 s if $t_p = 0.01$ s). Finally, we can combine these solutions, thus $T(x = 1, t) = b_0 - b_1$ (the alternating sign originates in $\cos(j\pi)$).

8.2. Step 2: solving the Guyer-Krumhansl equation. Here, we repeat the calculations using the same set of trial and weight functions for the GK model, that is, we solve

$$\partial_t T + \partial_x q = 0, \quad \tau_q \partial_t q + q + \alpha \partial_x T - \kappa^2 \partial_{xx} q = 0, \quad (30)$$

with

$$q_0(t) = -\left(\exp(-C_1 t/t_p) + \exp(-C_2 t/t_p)\right)/n, \quad q_1(t) = hT(x = 1, t), \quad q(x, t = 0) = 0, \quad T(x, t = 0) = 0. \quad (31)$$

Analogously with the Fourier case, we obtain a set of ODE as follows.

- For $j = 0$, we have

$$\dot{b}_0 + \partial_x w = 0, \rightarrow \dot{b}_0 = -hb_0 + q_0, \quad (32)$$

which is the same as previously due to $a_0 = 0$ identically.

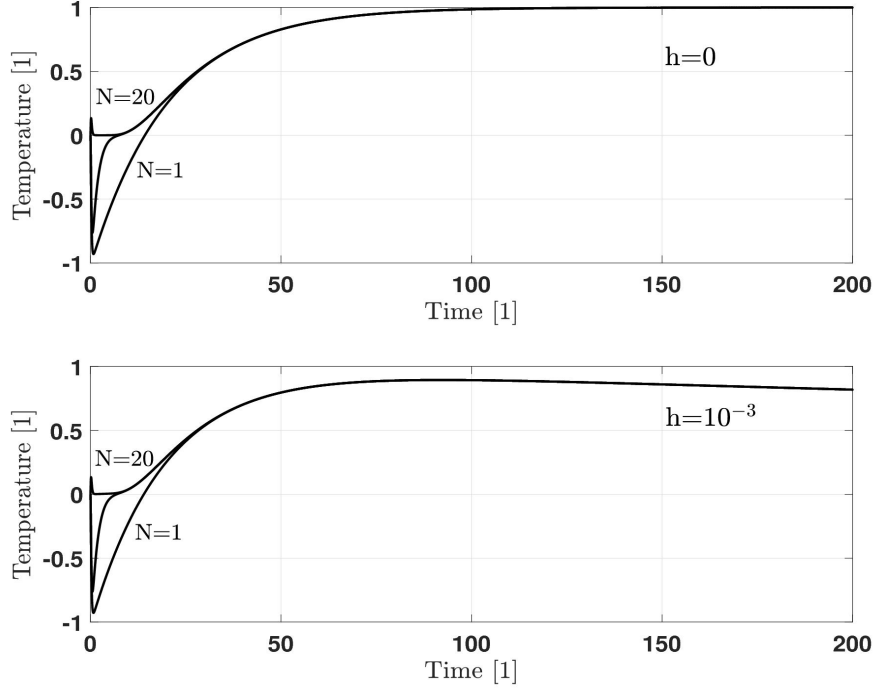


FIGURE 11. Convergence analysis for the Fourier equation in two different cases on the rear side temperature history. The first one shows the adiabatic limit, and the second one presents the case when the heat transfer coefficient h is not zero. In both cases, we applied 1, 3 and 20 terms in the spectral decomposition (24), with $\alpha = 0.005$.

- For $j > 0$, a_j changes

$$\dot{b}_j + j\pi a_j = 0, \quad (33)$$

$$\tau_q \dot{a}_j + (1 + \kappa^2 j^2 \pi^2) a_j = \alpha j \pi b_j + \frac{2}{j\pi} \left[(hb_j - q_0) + \tau_q (h\dot{b}_j - \dot{q}_0) \right]. \quad (34)$$

Consequently, the zeroth term, $b_0(t)$ remains the same with the particular solution being omitted,

$$b_0(t) = Y_0 \exp(-ht), \quad Y_0 = (C_1 - C_2) / (n(C_1 - h)(C_2 - h)). \quad (35)$$

However, for $b_1(t)$, the particular solution $P(t)$ becomes more important, its initial value influences the temperature history, i.e., $P_0 = P(t=0)$ and $DP_0 = d_t P(t=0)$ appears in the coefficients Z_1 and Z_2 , and the P_0 and DP_0 quantities are important in the evaluation method, too. Thus $b_1(t)$ reads

$$b_1(t) = Z_1 \exp(x_1 t) + Z_2 \exp(x_2 t) + P(t), \quad Z_1 = -\frac{DP_0 - P_0 x_2}{x_1 - x_2}, \quad Z_2 = -P_0 + \frac{DP_0 - P_0 x_2}{x_1 - x_2}. \quad (36)$$

The exponents x_1 and x_2 depend on the GK parameters τ_q and κ^2 , and obtained as the roots of the quadratic equation $x_j^2 + k_{1j}x + k_{2j} = 0$:

$$x_{1,2} = x_{j1,2} | j = 1, \quad x_{j1,2} = \frac{1}{2} \left(-k_{1j} \pm \sqrt{k_{1j}^2 - 4k_{2j}} \right), \quad k_{1j} = \frac{1 + \kappa^2 j^2 \pi^2}{\tau_q} + 2h, \quad k_{2j} = \frac{\alpha j^2 \pi^2}{\tau_q} + \frac{2h}{\tau_q}. \quad (37)$$

Furthermore, the particular solution reads as

$$P_j(t) = M_{j1} \exp(-C_1 t) + M_{j2} \exp(-C_2 t), \quad M_{j1} = \left(\frac{2C_1}{n} - \frac{2}{n\tau_q} \right) / [k_{2j} - k_{1j}C_1 + C_1^2],$$

$$M_{j2} = \left(-\frac{2C_2}{n} + \frac{2}{n\tau_q} \right) / [k_{2j} - k_{1j}C_2 + C_2^2]. \quad (38)$$

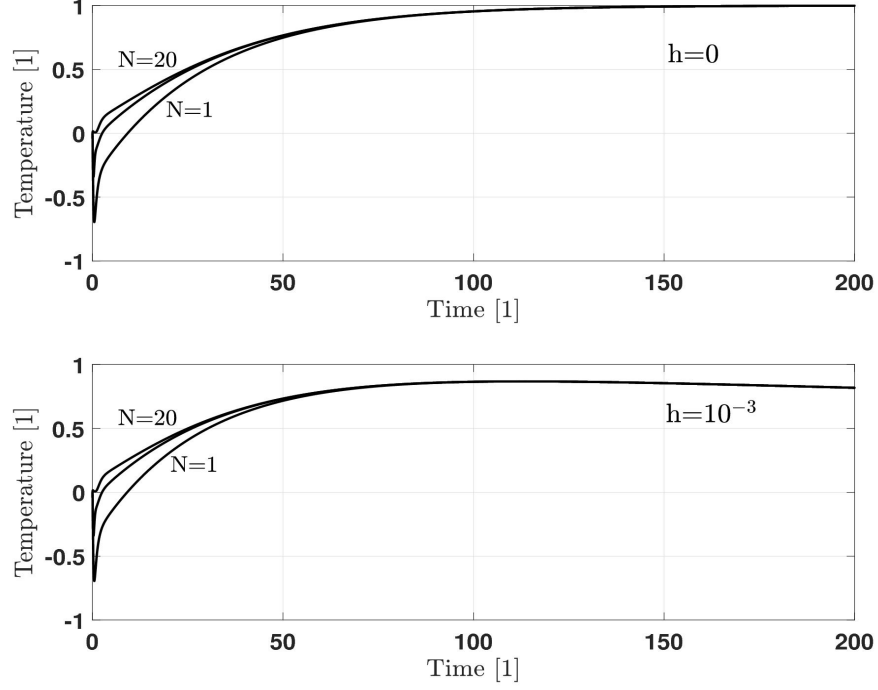


FIGURE 12. Convergence analysis for the Guyer-Krumhansl equation in two different cases on the rear side temperature history. The first one shows the adiabatic limit, and the second one presents the case when the heat transfer coefficient h is not zero. In both cases, we applied 1, 3 and 20 terms in the spectral decomposition (24), with $\alpha = 0.005$, $\tau_q = 1$, and $\kappa^2 = 10\alpha\tau_q$.

Hence $P_0 = M_1 + M_2$ and $DP_0 = -M_1C_1 - M_2C_2$ appears in $b_1(t)$ with $j = 1$, too. After obtaining Z_1 and Z_2 , $P(t)$ can be neglected since it becomes negligibly small at $t > t_p$. Finally, we formulate the rear side temperature history using $b_0(t)$ and $b_1(t)$ as

$$T(x = 1, t) = b_0 - b_1 = Y_0 \exp(-ht) - Z_1 \exp(x_1 t) - Z_2 \exp(x_2 t), \quad (39)$$

for which Figure 12 shows the convergence property.

REFERENCES

- [1] S. Both, B. Czél, T. Fülöp, Gy. Gróf, Á. Gyenis, R. Kovács, P. Ván, and J. Verhás. Deviation from the Fourier law in room-temperature heat pulse experiments. *Journal of Non-Equilibrium Thermodynamics*, 41(1):41–48, 2016.
- [2] P. Ván, A. Berezovski, T. Fülöp, Gy. Gróf, R. Kovács, Á. Lovas, and J. Verhás. Guyer-Krumhansl-type heat conduction at room temperature. *EPL*, 118(5):50005, 2017. arXiv:1704.00341v1.
- [3] T. Fülöp, R. Kovács, Á. Lovas, Á. Rieth, T. Fodor, M. Szücs, P. Ván, and Gy. Gróf. Emergence of non-Fourier hierarchies. *Entropy*, 20(11):832, 2018. ArXiv: 1808.06858.
- [4] P. Ván. Theories and heat pulse experiments of non-Fourier heat conduction. *Communications in Applied and Industrial Mathematics*, 7(2):150–166, 2016.
- [5] R. A. Guyer and J. A. Krumhansl. Solution of the linearized phonon Boltzmann equation. *Physical Review*, 148(2):766–778, 1966.
- [6] P. Ván. Weakly nonlocal irreversible thermodynamics – the Guyer-Krumhansl and the Cahn-Hilliard equations. *Physic Letters A*, 290(1-2):88–92, 2001.
- [7] P. Ván and T. Fülöp. Universality in heat conduction theory – weakly nonlocal thermodynamics. *Annalen der Physik (Berlin)*, 524(8):470–478, 2012.
- [8] L. Tisza. Transport phenomena in Helium II. *Nature*, 141:913, 1938.
- [9] L. Landau. On the theory of superfluidity of Helium II. *Journal of Physics*, 11(1):91–92, 1947.
- [10] R. A. Guyer and J. A. Krumhansl. Thermal Conductivity, Second Sound, and Phonon Hydrodynamic Phenomena in Nonmetallic Crystals. *Physical Review*, 148:778–788, 1966.
- [11] K. Mitra, S. Kumar, A. Vedevarz, and M. K. Moallemi. Experimental evidence of hyperbolic heat conduction in processed meat. *Journal of Heat Transfer*, 117(3):568–573, 1995.
- [12] V. Józsa and R. Kovács. *Solving Problems in Thermal Engineering: A Toolbox for Engineers*. Springer, 2020.
- [13] R. Kovács and P. Ván. Generalized heat conduction in heat pulse experiments. *International Journal of Heat and Mass Transfer*, 83:613 – 620, 2015.
- [14] W. Dreyer and H. Struchtrup. Heat pulse experiments revisited. *Continuum Mechanics and Thermodynamics*, 5:3–50, 1993.
- [15] I. Müller and T. Ruggeri. *Rational Extended Thermodynamics*. Springer, 1998.
- [16] D. Y. Tzou. Longitudinal and transverse phonon transport in dielectric crystals. *Journal of Heat Transfer*, 136(4):042401, 2014.
- [17] S. A. Rukolaine. Unphysical effects of the dual-phase-lag model of heat conduction. *International Journal of Heat and Mass Transfer*, 78:58–63, 2014.
- [18] S. A. Rukolaine. Unphysical effects of the dual-phase-lag model of heat conduction: higher-order approximations. *International Journal of Thermal Sciences*, 113:83–88, 2017.
- [19] M. Fabrizio, B. Lazzari, and V. Tibullo. Stability and thermodynamic restrictions for a dual-phase-lag thermal model. *Journal of Non-Equilibrium Thermodynamics*, 2017. Published Online:2017/01/10.
- [20] M. Fabrizio and F. Franchi. Delayed thermal models: stability and thermodynamics. *Journal of Thermal Stresses*, 37(2):160–173, 2014.
- [21] B. Nyíri. On the entropy current. *Journal of Non-Equilibrium Thermodynamics*, 16(2):179–186, 1991.
- [22] R. Kovács. Analytic solution of Guyer-Krumhansl equation for laser flash experiments. *International Journal of Heat and Mass Transfer*, 127:631–636, 2018.
- [23] T. Fülöp, R. Kovács, and P. Ván. Thermodynamic hierarchies of evolution equations. *Proceedings of the Estonian Academy of Sciences*, 64(3):389–395, 2015.
- [24] K. Zhukovsky. Violation of the maximum principle and negative solutions for pulse propagation in Guyer–Krumhansl model. *International Journal of Heat and Mass Transfer*, 98:523–529, 2016.
- [25] K. V. Zhukovsky. Exact solution of Guyer–Krumhansl type heat equation by operational method. *International Journal of Heat and Mass Transfer*, 96:132–144, 2016.
- [26] Á. Rieth, R. Kovács, and T. Fülöp. Implicit numerical schemes for generalized heat conduction equations. *International Journal of Heat and Mass Transfer*, 126:1177 – 1182, 2018.

¹DEPARTMENT OF ENERGY ENGINEERING, FACULTY OF MECHANICAL ENGINEERING, BME, BUDAPEST, HUNGARY ²DEPARTMENT OF THEORETICAL PHYSICS, WIGNER RESEARCH CENTRE FOR PHYSICS, INSTITUTE FOR PARTICLE AND NUCLEAR PHYSICS, BUDAPEST, HUNGARY ³MONTAVID THERMODYNAMIC RESEARCH GROUP